

Design and implementation of a digital MPPT controller for a photovoltaic panel

Djamel Eddine TOURQUI^{1,*}, Achour BETKA², Atallah SMAILI¹,
Tayeb ALLAOUI¹

¹L2GEGI, Laboratory of Energy Engineering and Computer Engineering, Tiaret, Algeria

²LGEB, Laboratory of Electrical Engineering, Biskra, Algeria

Received: 05.03.2015

Accepted/Published Online: 29.10.2015

Final Version: 06.12.2016

Abstract: This paper proposes a simplified design and hardware implementation of a digital maximum power point tracking (MPPT) controller for a photovoltaic (PV) panel using PIC microcontroller 16F877A embedded technology. The 3 most well-known algorithms, perturb & observe, hill-climbing, and incremental conductance, are considered and analyzed from a practical implementation point of view. The control board was developed using simple circuits and tested under resistive load conditions lower than the load of the maximum power point. The MPPT controller proved its effectiveness, providing maximum power to the load under changing weather conditions.

Key words: Photovoltaic panel, maximum power point, maximum power point tracking, PIC 16F877A, perturb & observe, hill-climbing, incremental conductance.

1. Introduction

Solar energy is among the most widely used renewable energy sources worldwide with a global installed capacity reaching 100 GW [1]. This source is considered as one of the best and most promising of alternative energy sources due to its natural availability and cleanliness [2,3].

Photovoltaic (PV) panels have a nonlinear voltage-current (I-V) characteristic with a unique point where the power generated is maximum. This is known as the maximum power point (MPP) at which the PV system operates at its highest efficiency. This point, located on the “knee” of the I-V curve, depends on the ambient temperature, T_{amb} , of the panel as well as the irradiance of the sun, E , which changes during the day.

One of the first difficulties associated with the use of a PV panel is the nonperfect coupling between the PV generator and the load [4]. One technological barrier that exists in this type of coupling is the problem of transferring the maximum power of the PV generator to the load, which often suffers from poor adaptation. The resulting operating point is then sometimes very far from the actual MPP. In other words, under these conditions it becomes difficult to extract the maximum output power from the PV panel under all weather conditions [5].

Consequently, a maximum power point tracking (MPPT) strategy is required to automatically find the PV panel’s operating voltage that produces the maximum power output [6]. There has been extensive research in this area and various methods exist in the literature, ranging from the simplest methods, such as perturb & observe (P&O) and incremental conductance (IncCond), to more sophisticated and complex ones [7–9].

*Correspondence: tourqui.djamel@gmail.com

The objective of static converters is to adapt the electrical energy from the PV panel to the load [10]. This adaptation can be achieved by inserting a DC-DC converter (chopper) controlled by a MPPT mechanism. Figure 1 represents the basic configuration of a PV power system with a MPPT mechanism.

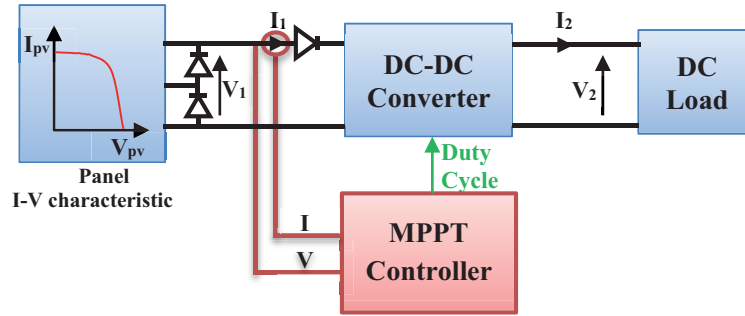


Figure 1. Elementary components of a PV power system.

The aim of this work is to implement 3 MPPT algorithms (P&O, hill-climbing, and IncCond), using a PIC microcontroller. The rest of the paper is organized as follows: Section 2 presents an overview of the modeling of a PV generator and the influence of E and T_{amb} on the electrical characteristics I-V. Section 3 overviews the different types of MPPT algorithms considered in this paper. Section 4 describes the hardware set-up of the various PV system components and the real-time programs that implement the MPPT algorithms on the microcontroller. Section 5 presents the experimental results and discussions. Finally, the conclusions and future actions are summarized in Section 6.

2. The PV generator model

The PV generator model is used to calculate the output power of the PV panels [11] under any temperature and irradiance conditions. A solar cell equivalent electrical circuit can be represented by a single-diode model as shown in Figure 2. The relationship between the cell terminal current I and voltage V is given by [12,13]:

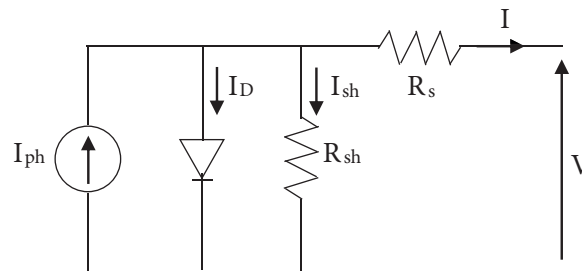


Figure 2. Equivalent circuit of the PV generator.

$$I = I_{ph} - I_D \left[\exp \left(\frac{V + R_s \times I}{m \times K_B \times T_{amb}} \right) - 1 \right] - \frac{V + R_s \times I}{R_{sh}} \quad (1)$$

It is known that the I-V characteristics (Figure 1) of a PV cell strongly depend on E and T_{amb} [14], so we will look for the model that gives the mathematical relationship between them. The analysis begins with calculating the module temperature T_m using the empirical model developed by Garcia and Balenzatgui [11,15] as follows:

$$T_m = T_{amb} + \frac{(NOCT - 20) E}{800} \tag{2}$$

The output power P is calculated based on the model developed by Skoplaki and Palyvos [16] as follows:

$$P = E \times A \times \eta T_{ref} (1 - B_{ref} (T_m - 25)). \tag{3}$$

3. Overview of MPPT algorithms

Several MPPT techniques have been reported in the literature. Examples can be found in [8,18,19]. The P&O, hill-climbing, and IncCond methods are the most widely used because of their simplicity and ease of implementation. The principles of these 3 algorithms are briefly summarized below.

3.1. Perturb and observe (P&O)

The P&O method is widely adopted for searching for the MPP because it is simple and requires only measurements of the voltage (V_{PV}) and current (I_{PV}) of the PV panel. P&O operates by periodically perturbing the control variable (say, voltage V_{PV}) and comparing the instantaneous powers P_{PV} before and after the perturbation [18,20,21]. If the change in output power dP_{PV} increases, V_{PV} is adjusted in the same direction as in the previous cycle. If dP_{PV} is negative, this means that the system is operating far from the optimal point, and thus the perturbation size needs to be reduced in order to bring the operating point back to the MPP [22]. Figure 3 shows the flowchart describing the implementation steps of the P&O algorithm.

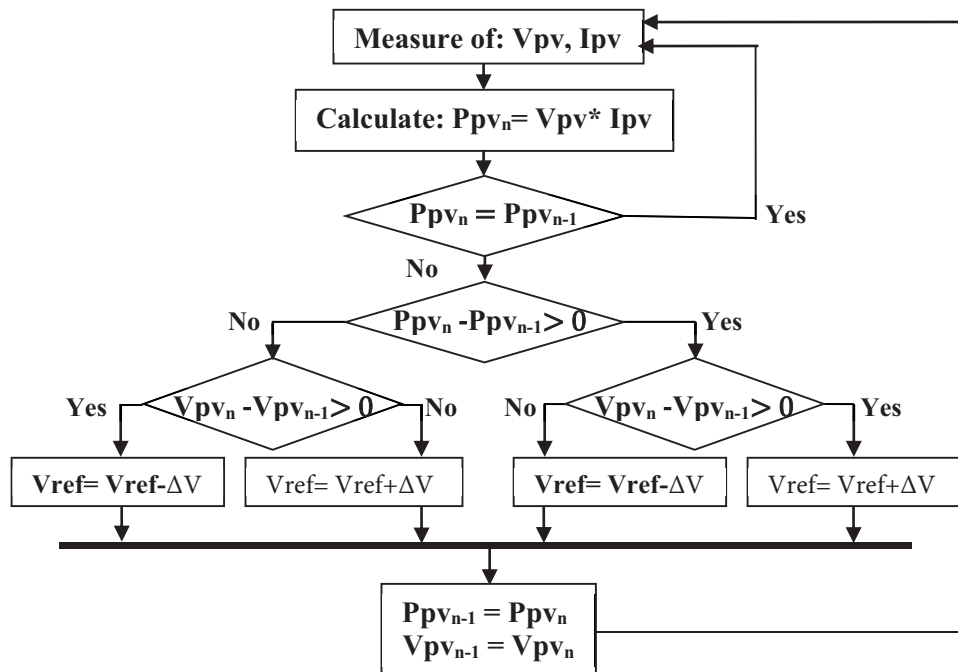


Figure 3. MPPT control algorithm based on P&O.

3.2. Hill-climbing method

Similarly to P&O, the hill-climbing method [18,23] consists of moving the operating point on the I-V curve in the direction in which the instantaneous power increases. In this case, the perturbation is applied to the duty cycle, D , of the DC-DC converter. The switching D of the power converter keeps changing until the operating power oscillates at the MPP [24,25]. A flow chart of the hill-climbing algorithm is shown in Figure 4.

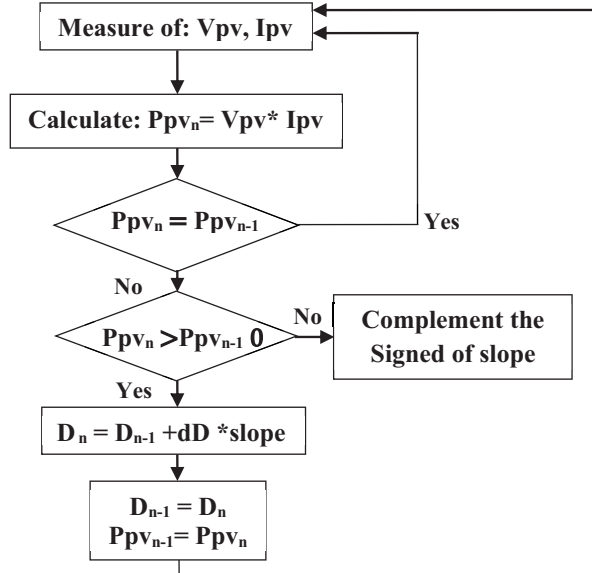


Figure 4. MPPT control algorithm based on hill-climbing.

3.3. Incremental conductance (IncCond)

To find the MPP, this technique uses the knowledge of the conductance variation of the PV panel (G) and the relative position of the operating point with respect to the MPP [26,27]. Consider the PV panel power curve of Figure 5.

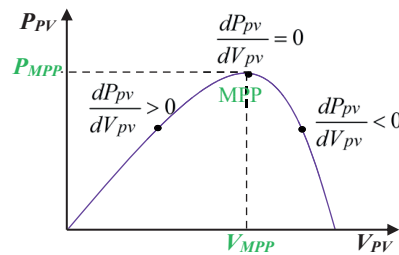


Figure 5. PV power characteristic for different operating points.

The equation for PV panel power is:

$$P_{pv} = V_{pv} \times I_{pv}, \tag{4}$$

$$\begin{cases} \frac{dP_{pv}}{dV_{pv}} = \frac{d(V_{pv} \times dI_{pv})}{dV_{pv}} \\ \frac{dP_{pv}}{dV_{pv}} = I_{pv} + V_{pv} \frac{dI_{pv}}{dV_{pv}} \\ \frac{1}{dV_{pv}} \times \frac{dP_{pv}}{dV_{pv}} = \frac{I_{pv}}{V_{pv}} + \frac{dI_{pv}}{dV_{pv}} \end{cases}, \tag{5}$$

where

$$P_{pv} = P_{pv_n} - P_{pv_{n-1}}, dV_{pv} = V_{pv_n} - V_{pv_{n-1}}, \text{ and } dI_{pv} = I_{pv_n} - I_{pv_{n-1}}. \quad (6)$$

The conductance G of the PV circuit is:

$$G = I_{pv}/V_{pv}. \quad (7)$$

Moreover, an elementary variation (increment) conductance can be defined by:

$$dG = dI_{pv}/dV_{pv}. \quad (8)$$

The basic concept of the IncCond method consists of comparing the evolution of the power module (dP_{PV}) with respect to the voltage (dV_{PV}) to determine in which direction the perturbation should be applied in order to shift the operating point towards the MPP (Figure 6) with reference to Figure 5. When the derivative of the power is zero, the operating point coincides with the MPP. This leads to a positive gradient on the left of the MPP and a negative gradient on the right of the MPP [25].

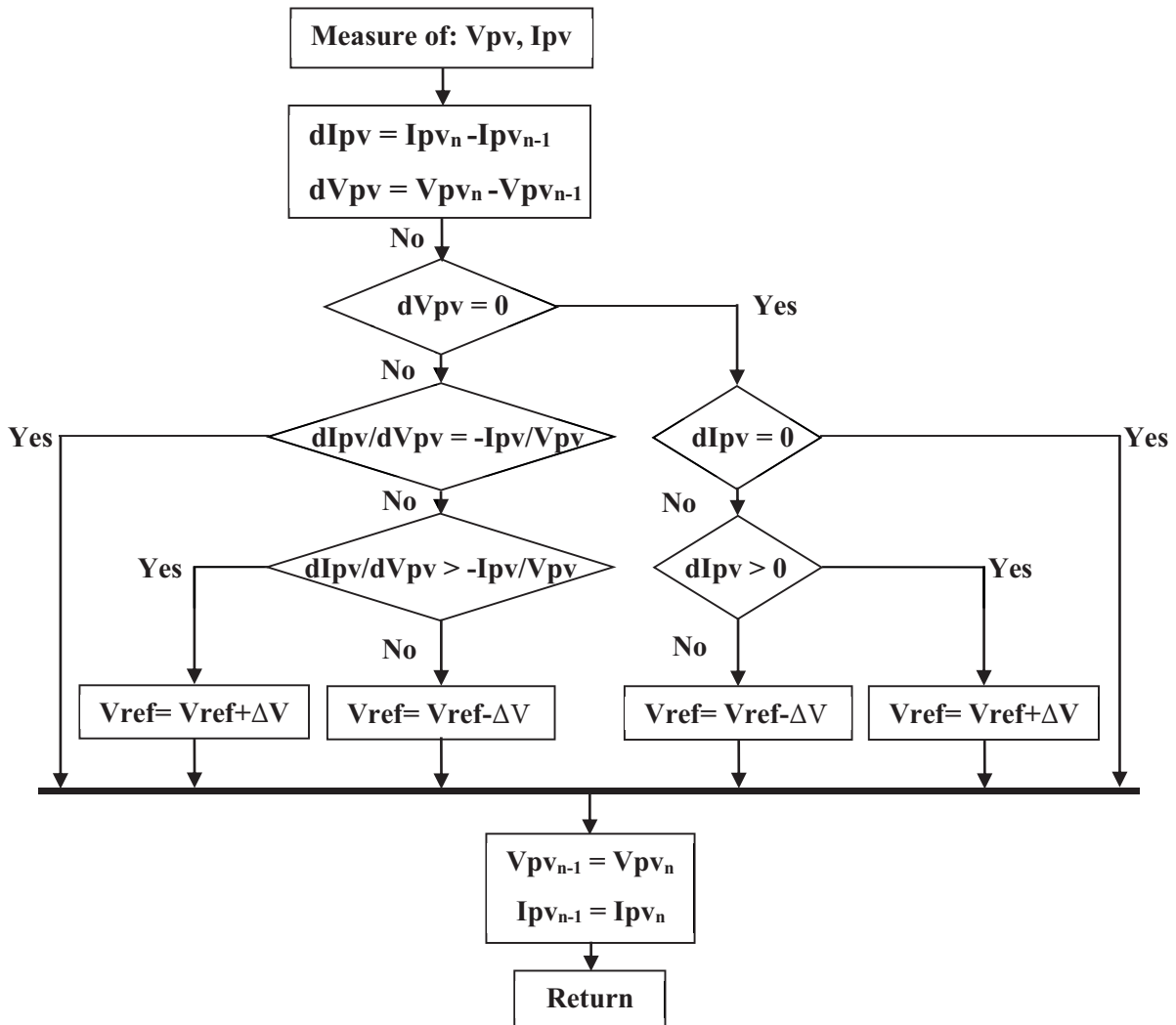


Figure 6. MPPT control algorithm based on IncCond.

The power gradients can be written as:

$$dP_{pv}/dV_{pv} = 0 \quad \text{at the MPP,} \tag{9}$$

$$dP_{pv}/dV_{pv} > 0 \quad \text{at t left of the MPP,} \tag{10}$$

$$dP_{pv}/dV_{pv} < 0 \quad \text{at the right of the MPP.} \tag{11}$$

4. Design and implementation of system

In this section, the design and implementation of the above MPPT algorithms on a PIC microcontroller is described. This microcontroller-based MPPT has several advantages compared to its analog counterpart [28,29]. The system consists of 3 blocks: the control block, power block, and energy block.

4.1. The control block

This has 2 main parts; the first includes an analog current sensor from a shunt resistor and a voltage sensor based on a voltage divider. The second part includes the control unit, a microcontroller that hosts the MPPT control algorithms. After isolation and amplification, the control signal (duty cycle) is sent to the power block.

4.2. The power block

This consists of a DC-DC buck converter, based on IGBT BUP 314, ensuring the transfer of all of the power extracted from the solar panel to a resistive load. The 80-W PV panel used in this study is shown in Figure 7. The buck converter is operated in continuous conduction mode (CCM) and the circuit parameters are $L = 600 \mu\text{H}$, $C1 = 2200 \mu\text{F}$, PV input capacitor $C2 = 200 \mu\text{F}$, and a diode, D1, forms the static buck converter. The value of inductor L was chosen to keep the converter operating in the CCM according to [30]:

$$L > \frac{V_{pv}}{4 \times dIL \times f}. \tag{12}$$



Figure 7. PV module employed in the experiment.

4.3. The energy block

This provides a stabilized voltage at $\pm 15 \text{ V}$ and $+5 \text{ V}$ levels to the different parts of the control circuit including the microcontroller, current sensor, and the optocoupler (type 4N25) used as the driver for the power switch to ensure galvanic isolation between the power and the control units.

The circuit model implemented using Proteus PCB design software is shown in Figure 8.

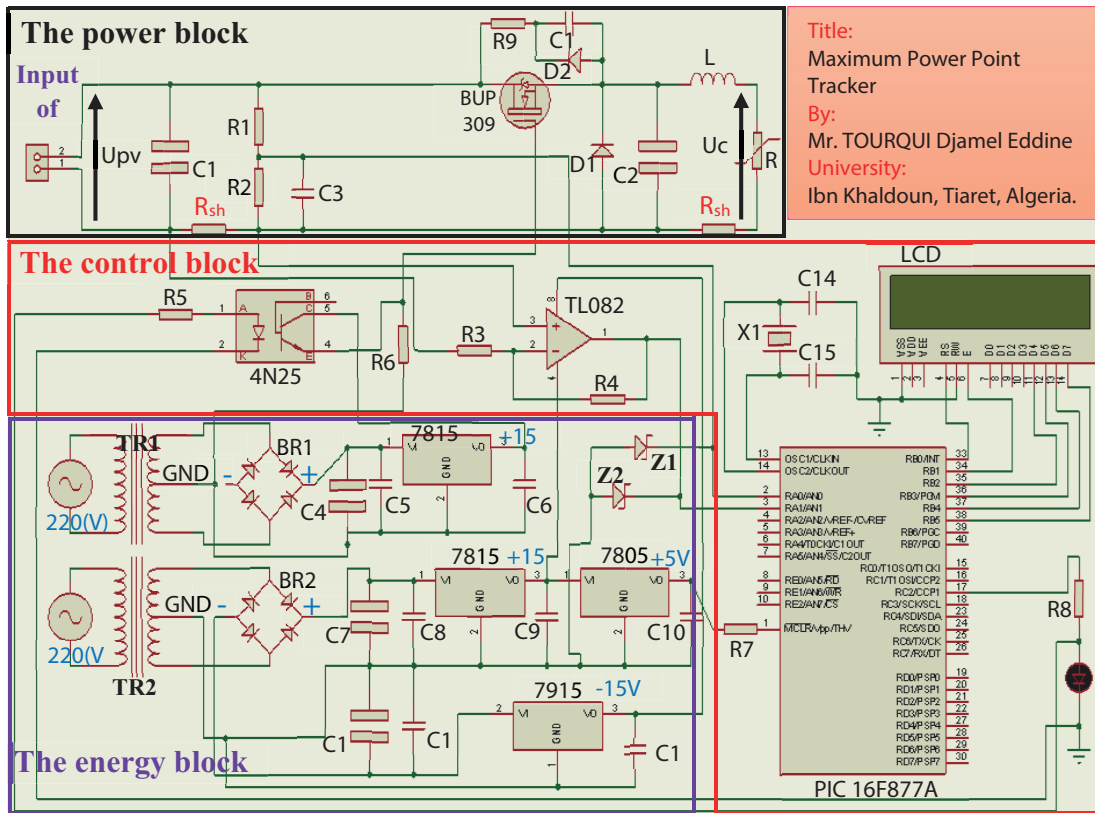
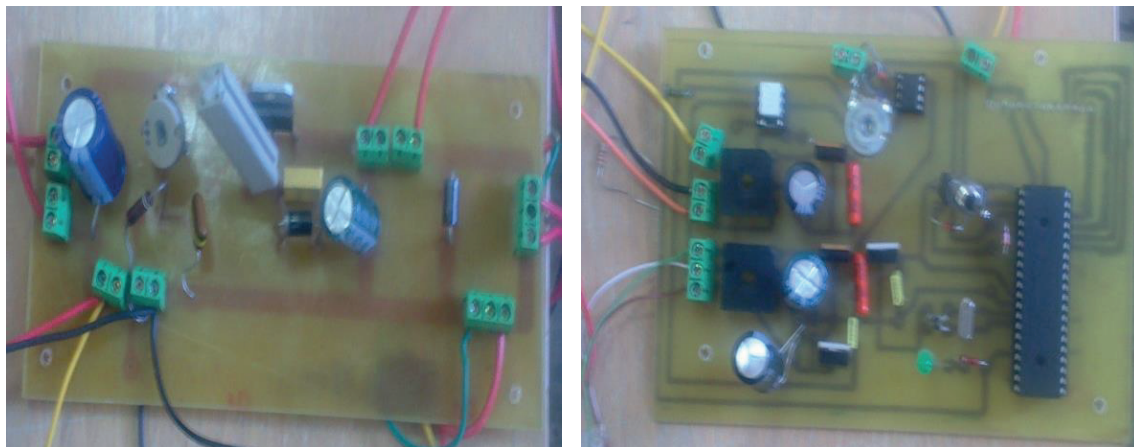


Figure 8. Complete wiring diagram of the prototype to achieve.

Figure 9a shows the actual experimental electronic cards of the power block of the digital MPPT controller and Figure 9b shows the electronic cards of the control block and energy block.



(a) Electronic cards of the power block.

(b) Electronic cards of the control block and energy block.

Figure 9. Practical realization of the electronic cards.

5. Performance evaluations and results

The experimental tests presented were performed on 3 clear days in 2013 and under the following operating conditions: a) direct coupling of the load on the panel without MPPT, b) with digital MPPT (DMPPT), and c) with manual MPPT for extracting the MPP (manual adaptive load variation). The results are presented for load $R_1 = 3.1 (\Omega)$, which is less than the load of the MPP.

As discussed previously, the characteristic I-V shows that the maximum power generated depends strongly on intensity E and T_{amb} . Therefore, we recorded measurements for P , E , and T_{amb} for each of the 3 of algorithms studied (P&O, hill-climbing, and IncCond) and the results are presented in Tables 1–3 respectively.

Table 1. Experimental values extracted by P&O algorithm.

Time (hh:mm)	P with direct coupling (w)	P with <i>DMPPT</i> (w)	P at <i>MPP</i> (w)	η (%)	E (w/m ²)	T (°C)
10:10	18	43	43	100	672	35.6
11:20	25	54	54	100	809	39.3
15:45	12	40	41	97.5	546	39.5
16:11	9	35	35	100	466	35.5
16:30	6	31	32	96.8	404	34.5

Table 2. Experimental values extracted by hill-climbing algorithm.

Time (hh:mm)	P with direct coupling (w)	P with <i>DMPPT</i> (w)	P at <i>MPP</i> (w)	η (%)	E (w/m ²)	T (°C)
09:58	14	39	42	92.8	547	41.5
10:55	18	48	49	97.9	697	44.3
11:27	22	52	52	100	749	46.5
12:10	22	52	53	98.1	774	45.5
13:50	20	47	47	100	686	45.5

Table 3. Experimental values extracted by IncCond algorithm.

Time (hh:mm)	P with direct coupling (w)	P with <i>DMPPT</i> (w)	P at <i>MPP</i> (w)	η (%)	E (w/m ²)	T (°C)
13:05	27	54	54	100	774	39.3
13:55	22	53	53	100	835	41
14:25	21.5	54	54	100	772	42
14:46	18	50	50	100	715	45.5
15:12	15	45	45.5	98.9	645	45.5

The histograms of Figures 10–12 for these 3 methods show the difference between the power in the case of direct coupling and the power recovered when applying digital MPPT control. This has also been compared with the manual search for the MPP.

Figures 13a–13d illustrate the current and voltage (U_{pv} , I_{pv}) of the PV generator and the current and voltage of the load (U_{ch} , I_{ch}) for the cases of direct coupling and P&O-based MPPT. The duty cycle signal of the converter in the case of the P&O algorithm is shown in Figure 14.

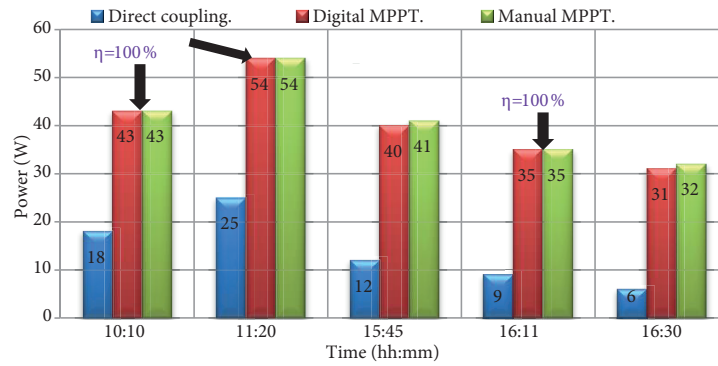


Figure 10. Histogram of powers to P&O algorithm.

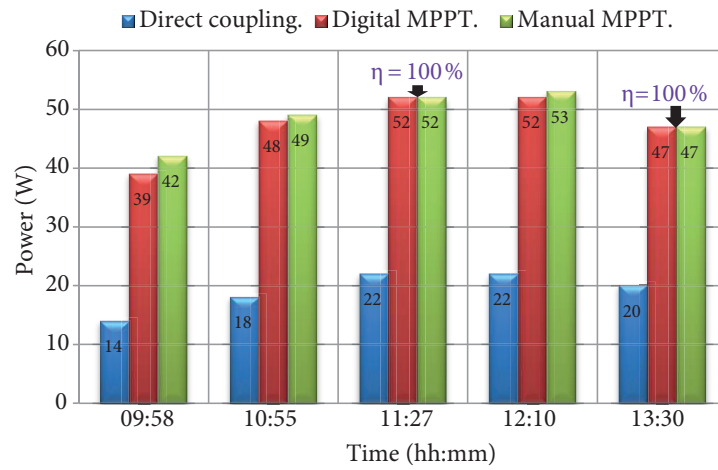


Figure 11. Histogram of powers to hill-climbing algorithm.

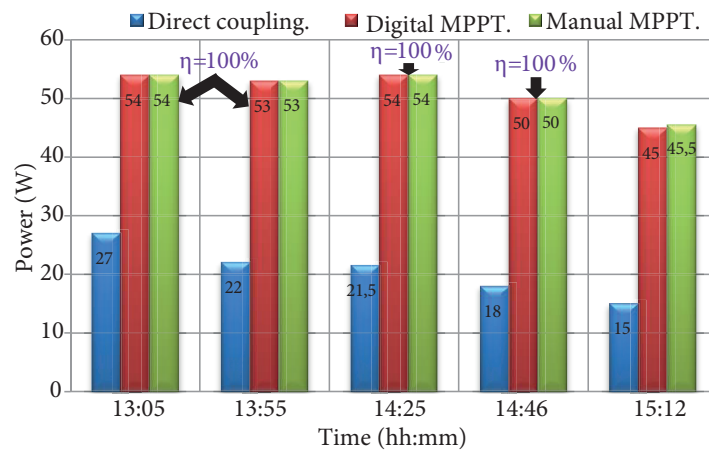
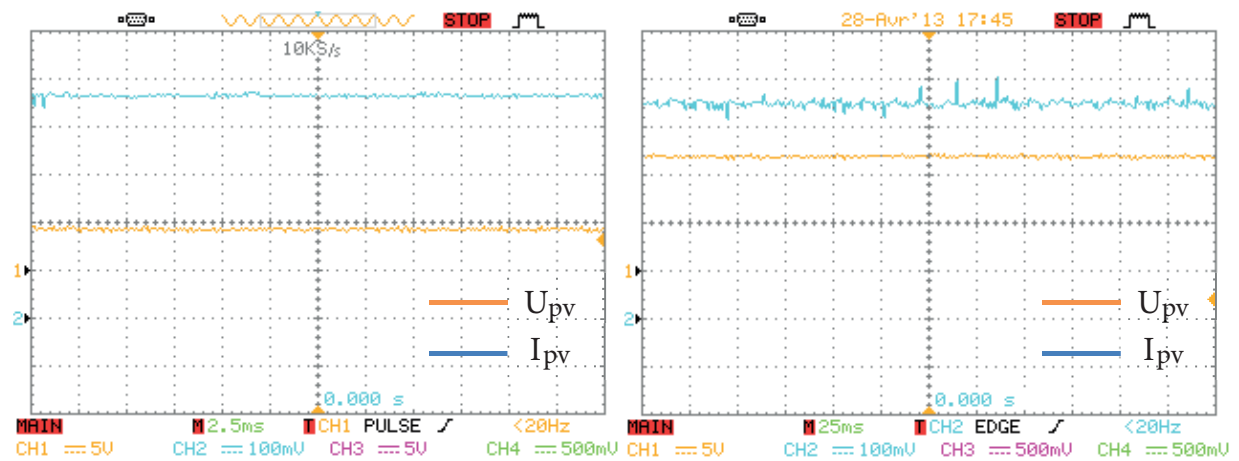


Figure 12. Histogram of powers to incremental conductance algorithm.

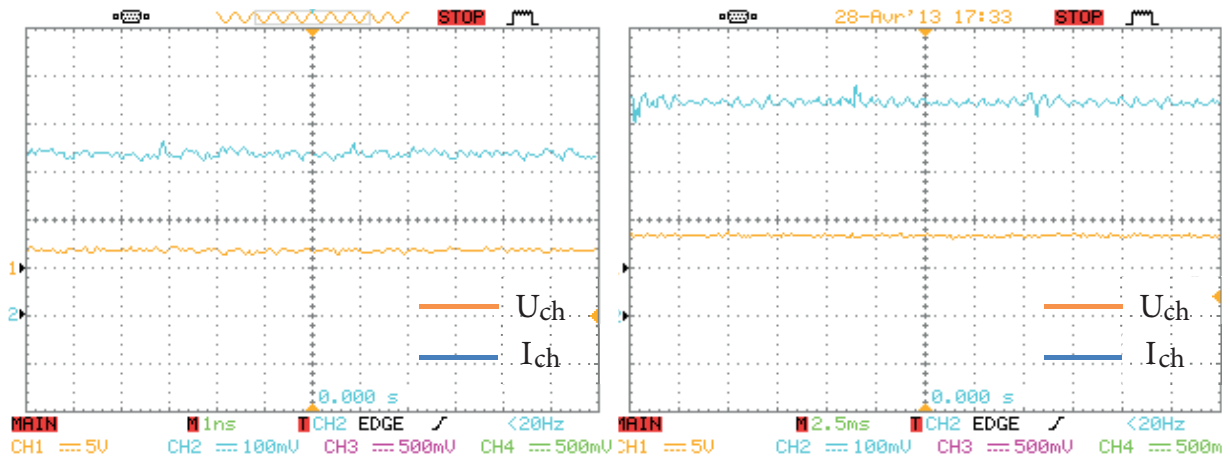
The results of current and voltage of the PV panel and the load obtained by the hill-climbing algorithm are shown in Figures 15a–15d. Figure 16 explains the duty cycle that controlled the DC-DC converter.

Finally, the same experiment is performed using IncCond control and the results are shown in Figures 17a–17d. Figure 18 shows the duty cycle generated by the IncCond algorithm.



(a): U_{pv} and I_{pv} with direct coupling

(b): U_{pv} and I_{pv} with digital MPPT.



(c): U_{ch} and I_{ch} with direct coupling

(d): U_{ch} and I_{ch} with digital MPPT.

Figure 13. Current and voltage of the studied system.

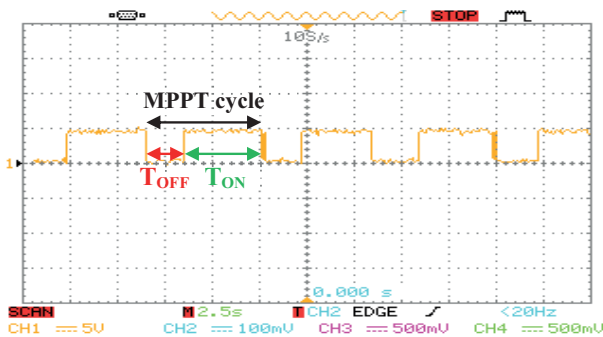


Figure 14. The duty cycle of the P&O algorithm.

5.1. Interpretation and discussion of the results

The experimental results (Tables 1–3) and the histograms (Figures 10–12) clearly demonstrate the effectiveness of the completed electronic card and the different methods used. With the digital MPPT the power delivered by

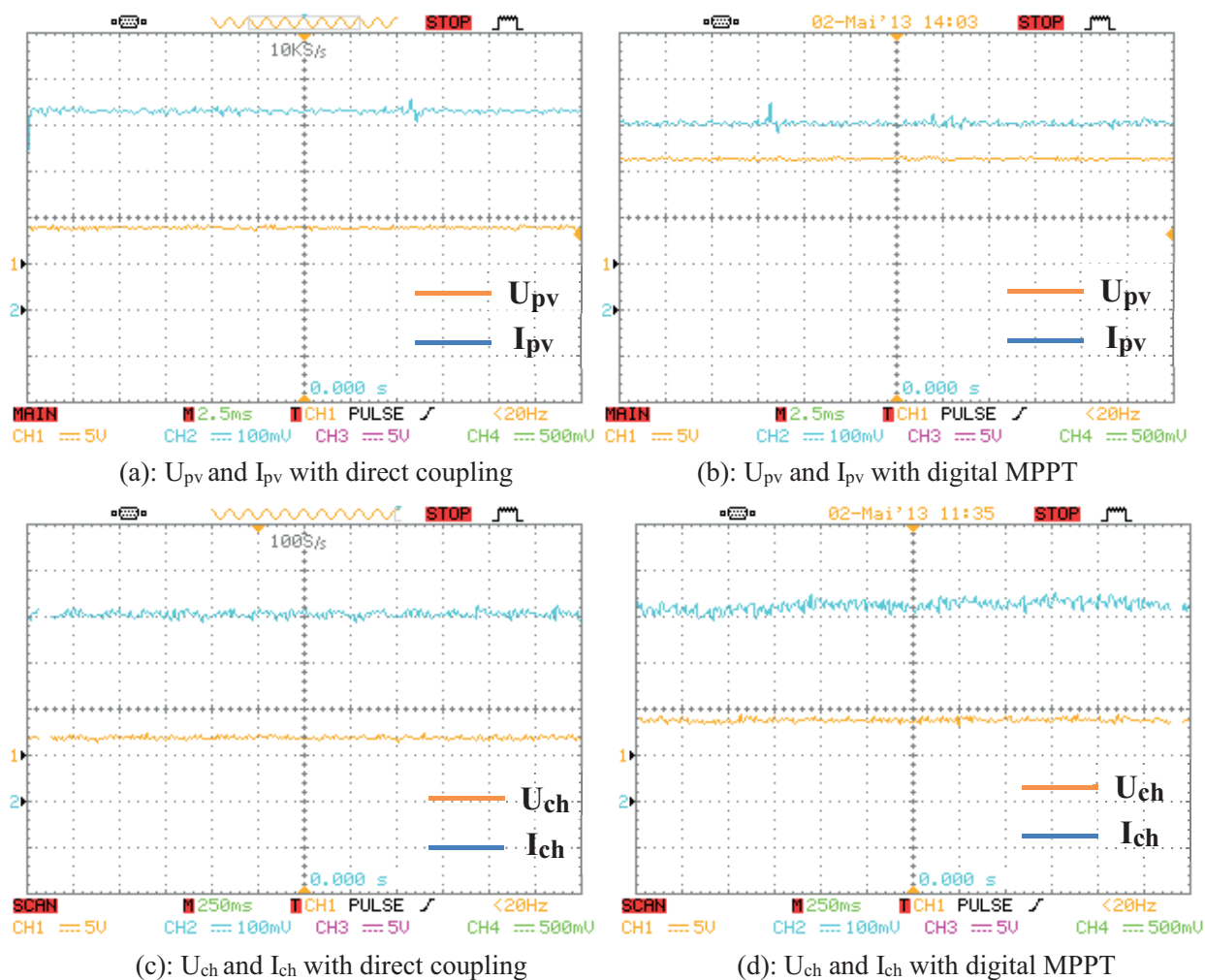


Figure 15. Current and voltage of the study system.

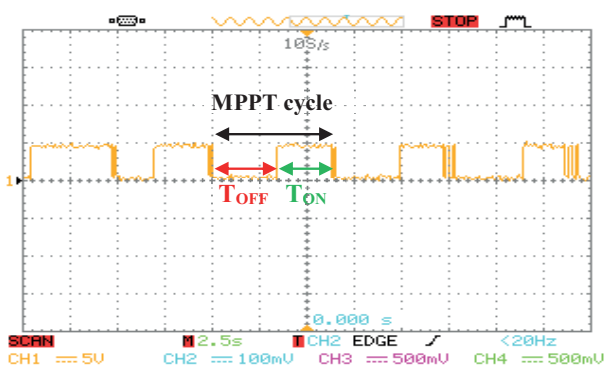


Figure 16. The duty cycle of the hill-climbing algorithm.

the PV generator is greater than the direct coupling with the load, so the presence of an adaptation between the PV panel and load reduces the losses caused by the direct connection. However, IncCond control was the most accurate and closest to the MPP compared to the hill-climbing and P&O methods and the results demonstrate a higher tracking efficiency of almost 100% between manual MPPT and digital MPPT in each of the 5 stages

of the experiment, where the tracking efficiency is defined as:

$$\eta(\%) = \frac{P_{DMPPT}}{P_{MPP}} \times 100 \tag{13}$$

where P_{DMPPT} represents the power reached by using the proposed DMPPT controller and P_{MPP} is the expected maximum power output at the MPP.

In Figures 13, 15, and 17, it can be seen that the buck converter operates in step-down voltage of the PV panel and the voltage V_{PV} stabilizes at 14.5 V. It can be noted that the load current operates in continuous conduction mode with a ripple at 2 kHz.

Finally, due to the integration of the PWM control signal in the PIC, the duty cycle generated by the digital MPPT (Figures 14, 16, and 18) have a frequency in the order of 2 kHz. If the V_{MPP} desired is higher than the V_{PV} measured, we increment the duty cycle; if not, we decrease it according to the command used. When adjusted in real time, this causes the operating point of the PV panel to oscillate around the MPP.

6. Conclusions and future actions

This paper presented a simplified design and implementation of an impedance matching stage using a DC-DC buck converter supplying a resistive load controlled by a low-cost microcontroller. This circuit allows the acquisition and processing of measured current and voltage signals and generates the appropriate control signals

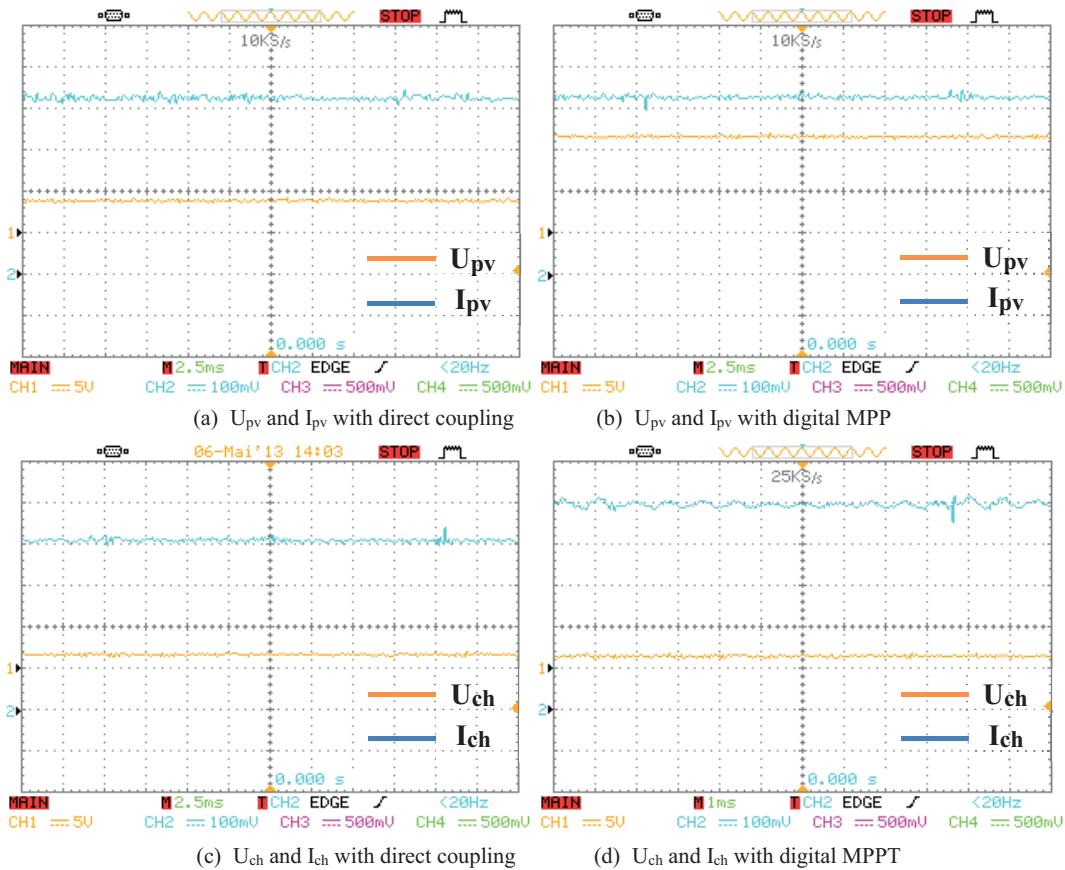


Figure 17. Current and voltage of the study system.

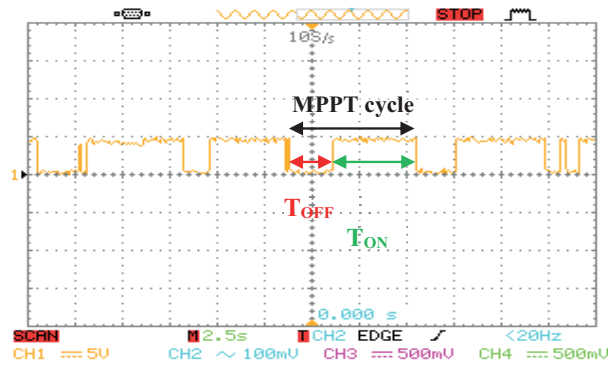


Figure 18. The duty cycle of the incremental conductance algorithm.

for controlling the switching of the power unit designed primarily around the buck converter. Three popular MPPT algorithms for extracting the maximum power of the photovoltaic panel, namely P&O, hill-climbing, and IncCond, were considered.

MPPT control led to improved speed of response, better MPP search accuracy, and good control in the presence of perturbations such as sudden variations of the illumination and temperature.

This work enables us to increase the cost-effectiveness of solar systems, as well as reducing the costs of imports from abroad both for our scientific laboratory and for the local sector using this energy to develop sustainable agriculture, such as photovoltaic pumping, irrigation, and domestic use.

Experiments with these prototypes on other PV installations (like the PV pumping available in our laboratory) will be presented in future works.

Nomenclature

I	output current
I_D	reverse saturation diode current
I_{ph}	photovoltaic current
K_B	Boltzmann constant ($1.3854 \times 10^{-23} \text{ J K}^{-1}$).
m	ideality factor.
NOCT	nominal operating.
q	charge of an electron ($1.6021 \times 10^{-19} \text{ C}$).
η_{Tref}	panel efficiency at the reference temperature.
A	area of solar cell.
B_{ref}	power temperature-coefficient, in the range of 0.22–0.71 (%/K).
dI_L	ripple current in inductor L .
f	switching frequency (Hz).
R_s	series resistance (Ω).
R_{sh}	shunt resistance (Ω).

References

- [1] Mellit A, Massi P A. Performance prediction of 20kWp grid-connected photovoltaic plant at Trieste (Italy) using artificial neural network. *Energ Convers Manage* 2010; 51: 2431-2441.
- [2] Parida B, Iniyar S, Goic R. A review of solar photovoltaic technologies. *Renew Sust Energ Rev* 2011; 15: 1625-1636.
- [3] Mellit A, Kalogirou SA, Hontoria L, Shaari S. Artificial intelligence techniques for sizing photovoltaic systems: a review. *Renew Sust Energ Rev* 2009; 13: 406-419.

- [4] Shraif MF. Optimisation et mesure de chaîne de conversion d'énergie photovoltaïque en énergie électrique. PhD, Paul Sabatier University, Toulouse, France, 2002 (in French).
- [5] Orabi M, Hilmy F, Shawky A, Jaber AAQ, Hasaneen E, Gomaa E. On-chip integrated power management MPPT controller utilizing cell-level architecture for PV solar system. *Sol Energy* 2015; 117: 10-28.
- [6] Sivakumar P, Abdullah AK, Yogeshraj K, Arutchelvi M. Analysis and enhancement of PV efficiency with incremental conductance MPPT technique under non-linear loading conditions. *Renew Energ* 2015; 81: 543-550.
- [7] Subudhi B, Pradhan R. A comparative study on maximum power point tracking techniques for photovoltaic power systems. *IEEE T Sust Energy* 2013; 4: 89-98.
- [8] ESRAM T, Chapman PL. Comparison of photovoltaic array maximum power point tracking techniques. *IEEE T Energy Convers* 2007; 22: 439-449.
- [9] De Brito MAG, Galotto L, Sampaio LP, de Azevedo e Melo G. Evaluation of the main MPPT techniques for photovoltaic applications. *IEEE T Ind Electron* 2013; 60: 1156-1167.
- [10] Learreta AB. Réalisation de commandes MPPT numériques. Report. Tarragona, Spain: Rovira i Virgili University, 2006 (in Spanish).
- [11] Sharaf Eldin SA, Abd-Elhady MS, Kandil HA. Feasibility of solar tracking systems for PV panels in hot and cold regions. *Renew Energ* 2016; 85: 228-233.
- [12] Ingegnoli A, Iannopolo A. A maximum power point tracking algorithm for stand-alone photovoltaic systems controlled by low computational power devices. In: 15th IEEE 2010 Mediterranean Electro-Technical Conference; 26–28 April 2010; Valletta, Malta. New York, NY, USA: IEEE. pp. 1522-1527.
- [13] Villalva MG, Gazoli JR, Ernesto RF. Comprehensive approach to modeling and simulation of photovoltaic arrays. *IEEE T Power Electr* 2009; 24: 1198-1208.
- [14] Nema P, Nema RK, Rangnekar S. A current and future state of art development of hybrid energy system using wind and PV-solar. *Renew Sust Energ Rev* 2009; 13: 2096-2103.
- [15] Garcia A, Balenzategui JL. Estimation of photovoltaic module yearly temperature and performance based on nominal operation cell temperature. *Renew Energ* 2004; 29: 1997-2010.
- [16] Skoplaki E, Palyvos JA. On the temperature dependence of photovoltaic module electrical performance. *Sol Energy* 2009; 83: 614-624.
- [17] Bücher K, Kleiss G, Dätzner D. Photovoltaic modules in buildings: performance and safety. *Renew Energ* 1998; 15: 545-551.
- [18] Cabal C. Optimisation énergétique de l'étage d'adaptation électronique dédié à la conversion photovoltaïque. PhD, Paul Sabatier III University, Toulouse, France, 2008 (in French).
- [19] Hohm DP, Ropp ME. Comparative study of maximum power point tracking algorithms using an experimental programmable maximum power point tracking test bed. In: IEEE 2000 Photovoltaic Specialists Conference; 15–22 September 2000; Anchorage, AK, USA. New York, NY, USA: IEEE. pp. 1699-1702.
- [20] Femia N, Petrone G, Spagnuolo G, Vitelli M. Optimization of perturb and observe maximum power point tracking method. *IEEE T Power Electr* 2005; 20: 963-973.
- [21] Sera D, Kerekes T, Teodorescu R, Blaabjerg F. Improved MPPT algorithms for rapidly changing environmental conditions. In: Power Electronics and Motion Control Conference 2006; 30 August–1 September 2006; Portoroz, Slovenia. New York, NY, USA: IEEE. pp. 1614-1619.
- [22] Onat N. Recent developments in maximum power point tracking technologies for photovoltaic systems. *Int J Photoenergy* 2010; 2010: 245316.
- [23] Xiao W, Dunford WG. Evaluating maximum power point tracking performance by using artificial lights. In: IEEE 2004 Industrial Electronics Society; 2–6 November 2004; Busan, Korea. New York, NY, USA: IEEE. pp. 2883-2887.

- [24] Shimizu TH, Kimura OG. A novel high performance utility interactive photovoltaic inverter system. *IEEE T Ind Electron* 2003; 18: 704-711.
- [25] Nur AK, Chee WT. A comprehensive review of maximum power point tracking algorithms for photovoltaic system. *Renew Sust Energ Rev* 2014; 37: 585-598.
- [26] Lee JH, Bae H, Cho BH. Advanced incremental conductance MPPT algorithm with a variable step size. In: *Power Electronics and Motion Control Conference 2006; 30 August–1 September 2006; Portoroz, Slovenia. New York, NY, USA: IEEE. pp. 603-607.*
- [27] Kim TY, Ahn HG, Park SK, Lee YK. A novel maximum power point tracking control for photovoltaic power system under rapidly changing solar radiation. In: *IEEE 2001 International Symposium on Industrial Electronics; 12–16 June 2001; Busan, Korea. New York, NY, USA: IEEE. pp. 1011-1014.*
- [28] Oi A. Design and simulation of photovoltaic water pumping system. MSc, California Polytechnic State University, San Luis Obispo, CA, USA, 2005.
- [29] Pongratananukul N. Analysis and simulation tools for solar array power systems. PhD, University of Central Florida, Orlando FL, USA, 2005.
- [30] Chun S, Kwasinski A. Modified Regula Falsi optimization method approach to digital maximum power point tracking for photovoltaic application. In: *IEEE 2011 Applied Power Electronics Conference and Exposition; 6–11 March 2011; Fort Worth, TX, USA. New York, NY, USA: IEEE. pp. 280-286.*